Linear dependence of surface drag on surface viscosity

Coralie Alonso and Joseph A. Zasadzinski*
Departments of Chemical Engineering and Materials, University of California, Santa Barbara, California 93106-5080, USA
(Received 23 July 2003; revised manuscript received 21 November 2003; published 24 February 2004)

Flow at an air-water interface is limited by drag from both the two-dimensional surface and three-dimensional subphase. Separating these contributions to the interfacial drag is necessary to measure surface viscosity as well as to understand the influence of the interface on flow. In these experiments, a magnetic needle floating on a monolayer-covered air-water interface is put in motion by applying a constant magnetic force, F_m. The needle velocity varies exponentially with time, reaching a terminal velocity F_m/C, in which C is the drag coefficient. C is shown to be linearly proportional to the monolayer surface viscosity, η_s, for dipalmitoylphosphatidylcholine monolayers in the condensed phase by comparison to surface viscosity measured by channel viscometry.

DOI: 10.1103/PhysRevE.69.021602 PACS number(s): 68.15.+e, 83.10.−y

The study of the viscosity and flow behavior of Langmuir monolayers has a long history as monolayer rheology plays a crucial role in dynamic processes at gas-liquid interfaces in both technology and biology [1,2]. There are two broad categories of surface viscosity measuring devices. The first is based on measuring the response of a monolayer to a torsion pendulum or other oscillator [2–4]. The second category, typified by the canal viscometer, relies on measuring aspects of a surface pressure gradient induced flow. The surface shear viscosity is evaluated by comparing the flow to solutions of the Navier-Stokes equation appropriate to the geometry [2,5–8]. For these types of viscometers, it is often necessary to determine the flow profile of the monolayer, using tracer particles, fluorescence microscopy [7], or Brewster angle microscopy [9]. The variation in surface pressure in the canal viscometer also makes it difficult to assign a particular surface pressure to a given surface viscosity, especially at phase coexistence where large variations in monolayer morphology occur over small changes in surface pressure.

The magnetic needle viscometer, first developed by Shahin [10] and modified by Brooks *et al.* [11] and Ding *et al.* [12,13], is a relatively new method for measuring monolayer viscosity. Helmholtz coils with a controlled current apply a force to a magnetic needle floating on the monolayer, which drives the needle into motion. If the applied force is oscillatory, the complex shear modulus is determined from measurements of the in-phase and out-of-phase response of the resulting strain [11]. If the applied force is constant, the shear surface viscosity of the monolayer can be extracted from the terminal velocity of the needle [12,13]. The major benefit of both of these devices is that the surface properties can be measured at constant surface pressure.

To extract the surface viscosity (or complex shear modulus), the terminal velocity of the needle, v_f, was assumed to be linear in the surface viscosity, η_s, for a given applied force. This is the result for a simple two-dimensional Couette flow [11,13]. This simplified flow assumption has been called into question by a recent theoretical analysis for a needle dragged across a laterally infinite water pool whose depth is small compared to the needle length [14]. In this theory, the drag on the needle depends on the square root of the surface viscosity when the ratio of surface drag to subphase drag (Boussinesq number, Bo) is of order 1. The drag on the needle approaches a linear response only when $\mathrm{Bo} \gg 1$ [14,15]. However, in our experimental apparatus, the needle moves in a channel the width of which is similar in magnitude to the water depth [12,13], which should result in a stronger dependence of the drag on the surface viscosity. Hence, it is necessary to determine the dependence of the surface drag on the surface viscosity over a range of Bo.

The surface viscosity of lipid monolayers is a strong function of the area per molecule, A, at the interface. For lipid monolayers in the condensed phase, experimental values of the surface viscosity determined from surface pressure driven flow in a channel viscometer are well correlated by a free-area model [5,8,16–18]:

$$\ln \eta_s = \ln \eta_s^0 + B\frac{A_0}{A_f}. \tag{1}$$

The free surface area, A_f, is the difference between the area/molecule, A, and the minimum required area/molecule, A_0 (taken to be the limiting area/molecule in that phase): $A_f = A - A_0$ [5,18]. This model is the two-dimensional analog of the classic free volume model developed to describe liquid viscosities [16,17]. From this model, a wide range of surface viscosities can be correlated with just a few parameters over a wide range of Bo.

We developed a direct method of measuring the absolute drag on the magnetic needle to determine the drag coefficient for DPPC (1,2-dipalmitoyl-*sn*-glycero-3-phosphatidylcholine) monolayers. The drag coefficients measured with the magnetic needle viscometer were compared to literature values of DPPC surface viscosity as a function of molecular area. The measured drag coefficient is well correlated by the free area model [Eq. (1)] and gives the same dependence on the free area as the surface viscosity data of Sacchetti *et al.* [5]. This confirms that the drag coefficient is linearly propor-

*Author to whom correspondence should be addressed at Department of Chemical Engineering, University of California, Santa Barbara, CA 93106-5080. FAX: 805-893-4731. Email address: gorilla@engineering.ucsb.edu

tional to the surface viscosity of monolayers of lipids in the condensed phase over a wide range of Bo. Hence, for the drag on a magnetic needle in a channel, the flow is similar to two-dimensional Couette flow [11], and is linear in the surface viscosity for Bo>1.

DPPC was purchased from Avanti Polar Lipids (Alabaster, AL; purity>99%). Monolayers were formed by spreading the appropriate amount of a 1 mg/ml chloroform solution onto pure Millipore water (18 MΩ cm resistivity) in a custom-built Langmuir trough [13] maintained at 25 °C. The trough was positioned between two Helmholtz coils to create a homogenous magnetic field gradient at the air/water interface and thus a constant magnetic force, F_m, when interacting with the permanent magnet in the needle. A channel, 14 mm wide, formed by two glass plates, was made along the axis of the magnetic gradient to direct the magnetic needle across the trough. The magnitude of the magnetic field gradient was adjusted by varying the current in the coils via two power supplies. A video camera directly above the channel recorded the needle motion; the video signal was digitized and the needle velocity derived from these images. The terminal needle velocities used for measurements range from about 1–15 mm/s. The estimated shear rate (terminal velocity/channel half width) varies from about 0.01–2 s^{-1}. There was no variation in the measured surface drag over these shear rates. A more detailed description of the magnetic needle viscometer can be found in Ref. [13].

The motion of the needle results from the competition between the inertia due to the needle mass, *m*, the applied magnetic force, F_m, and the viscous drag force *F*, which is assumed to be linearly proportional to the needle velocity [13–15]:

$$F = -Cv \tag{2}$$

in which *C* is the drag coefficient. *C* contains contributions from the drag due to the monolayer and the subphase [13–15]. On application of the magnetic force, the needle moves according to the force balance,

$$m\frac{dv}{dt} = F_m - Cv, \tag{3}$$

the solution to which is

$$v = \frac{F_m}{C}(1 - e^{(-Ct/m)}). \tag{4}$$

Figure 1 shows the needle velocity profile at the air-water interface and the corresponding fit to Eq. (4). The needle does not move instantly when the magnetic field is switched on. Short-range capillary attraction (the characteristic length scale for capillary forces, $(\gamma/\Delta\rho g)^{1/2} \approx 2-3$ mm; γ is the surface tension, $\Delta\rho$ is the density difference between water and air, and g is gravity [19]) between the needle and the walls of the trough must be overcome before the needle can move according to Eq. (4) [19,20]. A delay time, t_0, was introduced as a fitting parameter to compensate for this behavior at small *t*. After t_0 the needle velocity is well described by Eq. (4), the average errors being less than 5%,

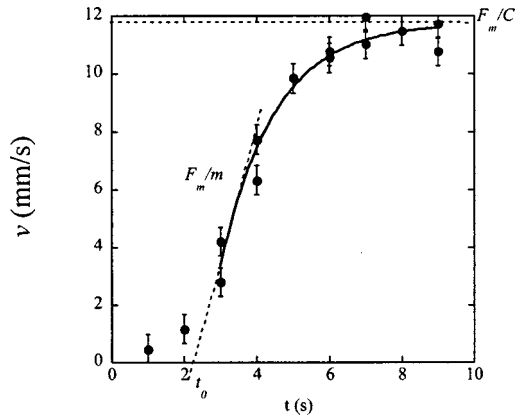

FIG. 1. Velocity profile of magnetic needle floating on bare water. The current applied in the Helmholtz coils was 1.4 V. The line is a fit to Eq. (4) after a lag time of $t_0 = 2.5 \pm 0.1$ s. The terminal velocity, $v_{f,} = 11.8 \pm 0.4$ mm/s $= F_m/C$, corresponding to a drag coefficient $C_w = 0.04 \pm 0.01$ mN s/m. The initial slope gives the ratio between the applied force and the needle mass, F_m/m.

justifying the assumption that the drag force is linearly proportional to the needle velocity. The terminal velocity and the startup velocity are determined from a fit to Eq. (4).

F_m is set by the interaction of a permanent magnet in the needle with a constant magnetic field gradient along the axis between two Helmholtz coils,

$$F_m = \eta\left(\frac{dB}{dx}\right) = \eta\frac{-3\mu_0 N R^2}{2}\left[\frac{xI_A}{(R^2+x^2)^{5/2}} - \frac{(L-x)I_B}{[R^2+(L-x)^2]^{5/2}}\right] \tag{5}$$

in which η is the magnetic dipole moment of the needle, μ_0 the permeability constant, *N* the number of turns in the coils, *R* the coil radius, I_A and I_B are the currents in the coils, and *x* is the distance from coil *A*. F_m is constant over the length of the needle channel if *L*, the distance between the coils, equals twice the radius, *R*, of the coils, and the same magnitude, but opposite direction current in the two coils $I_A = -I_B$, is applied. A Gauss meter was used to check the predictions of Eq. (5), which was valid within a few percent over the entire gap between the coils (data not shown). From Eq. (5), F_m is proportional to the magnitude of the applied current:

$$F_m = \kappa I_A. \tag{6}$$

κ is a parameter that depends on the needle size, shape, and magnet, but is independent of the subphase and monolayer. κ was determined from the asymptotic variation of v for t close to t_0:

$$v(t \to t_0) \cong \frac{F_m}{m}t. \tag{7}$$

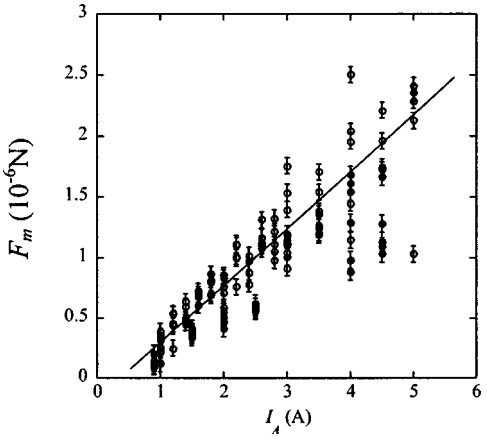

FIG. 2. Magnetic force, F_m, as a function of applied current for two interfaces, bare water (○) and a DPPC monolayer-covered interface at 20 mN/m and 25 °C (●). F_m varies linearly with the current, independent of the surface coverage, with an average slope $\kappa=0.35\pm0.02$ μN/A.

The slope of the needle velocity vs time curve (Fig. 1) for different applied currents (I_A) determines the relationship between F_m and I_A. F_m was evaluated according to Eq. (7) for bare water and for a DPPC monolayer in the liquid condensed (LC) phase as a function of I_A in Fig. 2. All the experimental points follow the same line with an average slope $\kappa=0.35$ μN/A for this needle (the offset from the origin is due to the time delay t_0). Knowing the absolute value of the magnetic force, F_m, the drag coefficient, $C=F_m/v_f$, can be calculated [Eq. (4)] from the terminal velocity, v_f, and checked for self-consistency. The measured values of C for a bare water and a DPPC monolayer covered interface were roughly Gaussian with their respective maxima at 0.04 and 0.11 mN s/m [21], independent of applied current from 1–5 A; the width of both distributions at half-maximum was about 0.01 mN s/m.

Although the phase behavior and structure of DPPC monolayers is well known [22–26], there are surprisingly few systematic measurements of DPPC surface shear viscosity over a wide range of Boussinesq number, Bo [5,8,18]. The most reliable data is probably that of Sacchetti *et al.* [5], who measured DPPC shear viscosity in the condensed phase using canal viscometry and correlated the data with a free area model [5]. An additional complication is that the canal viscometer requires a variation in surface pressure along the length of the channel to induce the flow [5]. Hence, the actual surface pressure (or area per molecule) at which the surface viscosity is being measured is more ambiguous than the experiments reported here. To minimize these effects, both surface viscosity and drag coefficient data were fit to the free area model [Eq. (1)] to determine the relationship between the experimentally measured absolute drag coefficients with surface viscosity.

From theory [11,14,15], the drag coefficient of a needle at an air-water interface covered by an insoluble monolayer should depend on the surface viscosity as a power law with exponent, $0\leqslant n\leqslant 1$, although n may vary depending on the Bo number [14].

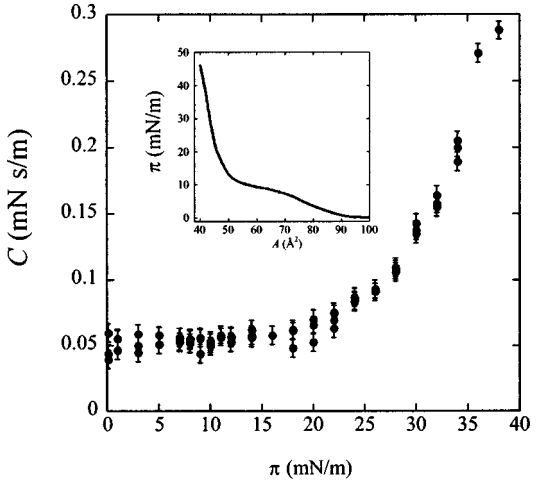

FIG. 3. Drag coefficient, C, as a function of surface pressure for a DPPC monolayer spread on water at 25 °C. The inset is an isotherm of DPPC at 25 °C showing the coexistence plateau at $\sim\pi=12$ mN/m separating the liquid expanded (LE) phase at low pressure and the liquid condensed (LC) phase at higher pressure.

$$C=\alpha\eta_s^n,$$

$$\eta_s=\left(\frac{C}{\alpha}\right)^{1/n}. \tag{8}$$

For n constant, C should obey the free area model of Eq. (1):

$$\ln\left(\frac{C}{\alpha}\right)^{1/n}=\ln\eta_s^o+B\frac{A_0}{A_f},$$

$$\ln C=\ln\alpha(\eta_s^o)^n+nB\frac{A_0}{A_f}, \tag{9}$$

$$\ln C=\ln C_w+nB\frac{A_0}{A_f}.$$

C_w is the drag on a bare water interface. Comparing Eq. (9) with Eq. (1) shows that the parameter B of the free area model for surface viscosity is simply related to that for the drag coefficient, $B=B'/n$, for constant n. For $n\cong 1$, $B\cong B'$.

Figure 3 shows the drag coefficient, C, for a DPPC monolayer on water at 25 °C as a function of the area per molecule A (A was determined from the isotherm at a given surface pressure, π). The plateau in the isotherm at $\sim$12 mN/m locates the first order phase transition between the liquid-expanded (LE) to the liquid condensed (LC) phase [24]. For π below the plateau, C is roughly constant at 0.05 mN s/m [21], slightly above that for the bare interface, C_w. In the LC phase, the drag coefficient increases steadily and the surface viscosity dominates the flow.

Figures 4 (top) and 4 (bottom) show the best fit of the free area model to the surface viscosity data of Sacchetti *et al.* [5] and the drag coefficient C measured with the magnetic needle. A_0, B (or B') and η_0 (or C_w) are determined from the fit of the data to Eq. (1) [Fig. 4 (top)] or Eq. (9) [Fig.

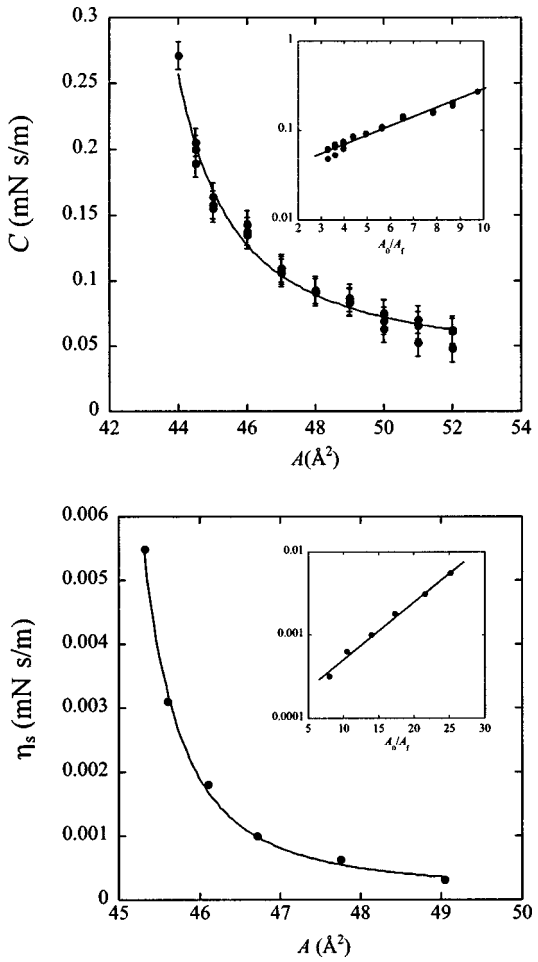

FIG. 4. (Top) C as a function of molecular area A. The solid line corresponds to the fit to the free area model, Eq. (9), with $C_w = 0.030 \pm 0.005$ mN s/m, $nB = 0.22 \pm 0.056$, and $A_0 = 39.9 \pm 0.7$ Å^2. The inset shows C as a function of the free area, $A_f = A - A_0$, calculated from the value of A_0 determined from the fit, confirming the constant power law relationship between the surface viscosity and the drag coefficient. (Bottom) Surface viscosity data from Sacchetti *et al.* as a function of molecular area A. The solid line corresponds to the fit to Eq. (1) with $\eta_0 = (7.9 \pm 5) \times 10^{-5}$ mN s/m, $B = 0.20 \pm 0.074$, and $A_0 = 43.2 \pm 0.4$ Å^2. nB is equal to B within experimental error confirming that the drag coefficient is linearly proportional to surface viscosity. The inset shows the free area model calculated from the value of A_0 determined from the fit.

4 (bottom)]. Both fits are very good suggesting that the free area model correlates both the surface viscosity and the absolute drag coefficient. This confirms that the drag coefficient can be expressed as a single power law in the surface viscosity over the range of Bo we examined here, $1 < \mathrm{Bo} < 10$. For the surface viscosity data of Sacchetti *et al.* [5], the best fit to Eq. (1) gives $\eta_0 = 7.9 \pm 5 \times 10^{-5}$ mN s/m, $B = 0.20 \pm 0.074$, $A_0 = 43.2 \pm 0.4$ Å^2. For our drag coefficient data, the optimal values of the fit to Eq. (9) are $C_w = 0.030 \pm 0.005$ mN s/m, $nB = 0.22 \pm 0.056$, and $A_0 = 39.9 \pm 0.7$ Å^2. The values of A_0 obtained are comparable to the expected values of 40–44 Å^2/mol obtained from various literature sources for DPPC [5,26,27], and the value of C_w is similar to

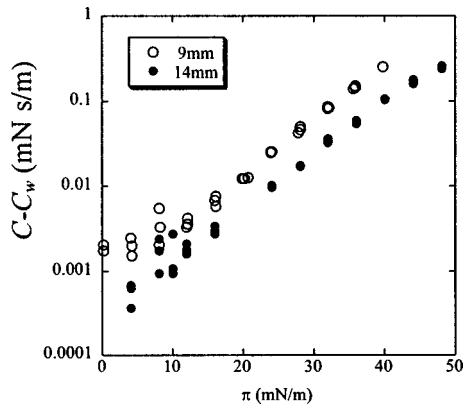

FIG. 5. Log plot of the drag coefficient for two different channel widths, 9 and 14 mm, for a DPPC monolayer as a function of surface pressure. The two lines are parallel showing that there is a constant factor of ~2.5 at all surface pressures for the narrow channel.

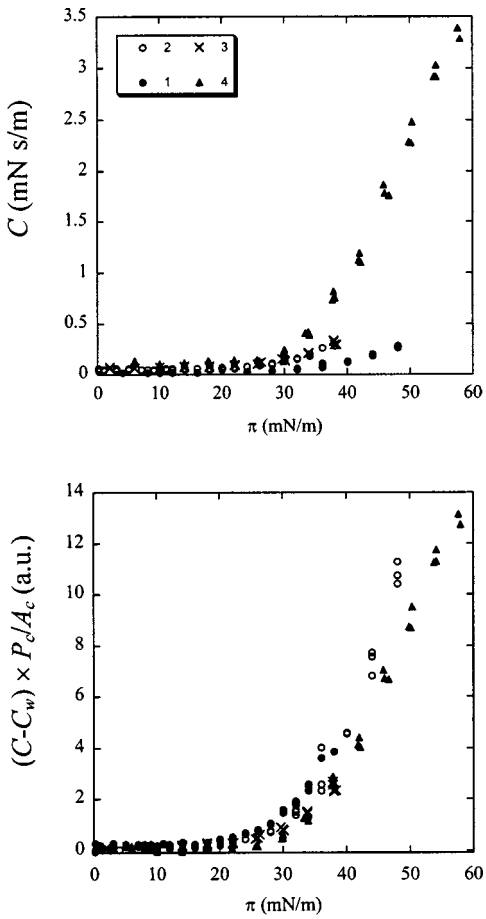

FIG. 6. Drag coefficient as a function of surface pressure for a monolayer of DPPC spread on water at 25 °C. Four needles with the same length but different diameters (1.4, 2.0, 2.3, 3.3 mm, respectively, for needle 1, 2, 3, 4) were used. (Top) Measured drag coefficient, C, for the different needles. (Bottom) $[(C - C_w)/C_w] \times (P_c/A_c)$ is plotted to correct for the effect of changing the needle dimensions. C_w is the drag for a bare water surface; P_c/A_c is the ratio of the needle perimeter to the contact area with the water subphase. The four curves superimpose.

that measured directly, 0.04 ± 0.01 mN s/m.

Within experimental error, $B = nB$, suggesting that the power law exponent is constant and equal to 1. Hence, the drag coefficient depends linearly on the surface viscosity for the Bo range of about 1 to about 10 for this experiment. As the approximation that the drag coefficient is linear in surface viscosity improves with increasing Bo, this means that the viscosity ratios measured in Ref. [12], in which $1 < \mathrm{Bo} < \sim 500$, are accurate.

From our results, it follows that Bo should give a good approximation of how C depends on the geometry of experiment and the needle diameter [11–13].

$$\mathrm{Bo} \equiv \frac{(\text{surface drag})}{(\text{subphase drag})} = \frac{\eta_s P_c / L_c'}{\eta A_c / L_c''} \propto \frac{(C - C_w) P_c / L_c'}{C_w A_c / L_c''}. \tag{10}$$

η is the subphase viscosity, L_c' and L_c'' are the characteristic length scales for shear in the surface and subphase, P_c is the contact perimeter between the needle and the interface, and A_c is the contact area between the needle and the subphase. Decreasing the channel width from 14 to 9 mm does not change P_c / A_c, but does increase L_c'' / L_c'. Hence, the measured drag coefficient at a given surface pressure (or equivalently, area per molecule) for the smaller channel should increase by the same ratio independent of the magnitude of the surface viscosity. Figure 5 shows $(C - C_w)$ for the narrow channel is consistently about 2.5 times that of $(C - C_w)$ for the wider channel over almost 3 decades in mN s/m. For a given channel width, P_c / A_c can be varied by changing the diameter of the needle. The surface drag for a DPPC monolayer was measured using four different needles of the same length (3 cm) but with diameters of 1.4, 2.0, 2.3, and 3.3 mm. As expected, the surface drag [Fig. 6 (top)] increases with the needle diameter and the scaling factor between needles is the ratio P_c / A_c [Fig. 6 (bottom)].

Characterizing the mechanical properties of complex monolayers is important to understanding the relationships between monolayer composition, structure, and function. The magnetic needle viscometer described here allows for quick measurements of the drag on a magnetic needle at a monolayer-covered interface at a known and constant surface pressure (or equivalent area/molecule). This is especially important to measure surface viscosity in the vicinity of first or second order phase transitions at which the properties of the monolayer may change dramatically with small changes in surface pressure [13]. Monolayers at coexistence can also be investigated with minimal disruption of the distribution of coexisting phases [12]. However, to analyze the data from the viscometer, it is important that the drag coefficient is simply related to the surface viscosity over the useful range of experimental parameters, especially Bo, the ratio of surface drag to subphase drag. We have shown that the drag coefficient is linearly related to the surface viscosity for $\mathrm{Bo} > 1$ by comparing surface viscosity data of DPPC from a channel viscometer with the absolute drag coefficient measured by our needle viscometer. All of the necessary instrumental parameters of the needle viscometer are measured directly, with no assumptions regarding the relationship between drag and surface viscosity. Hence, after calibration to known surface viscosities [13], the magnetic needle viscometer is a reliable method for measuring surface viscosity.

The authors acknowledge helpful discussions with J. Ding, D. K. Schwartz, Th. M. Fischer, and A. Levine. Financial support was provided from NIH Grant No. HL-51177 and the University of California Tobacco Related Disease Research Program, Grant No. 11RT-0222.

[1] D. A. Edwards, H. Brenner, and D. T. Wasan, *Interfacial Rheology: Basic Theory, Measurements and Applications* (Butterworth-Heinemann, Boston, MA, 1991).
[2] B. Kanner and J. E. Glass, Ind. Eng. Chem. **61**, 31 (1969).
[3] J. Kraegel, G. Kretzschmar, J. B. Li, G. Loglio, R. Miller, and H. Moehwald, Thin Solid Films **284-285**, 361 (1996).
[4] R. S. Ghaskadvi, T. M. Bohanon, P. Dutta, and J. B. Ketterson, Phys. Rev. E **54**, 1770 (1996).
[5] M. Sacchetti, H. Yu, and G. Zografi, Langmuir **9**, 2168 (1993).
[6] M. Sacchetti, H. Yu, and G. Zografi, Rev. Sci. Instrum. **64**, 1941 (1993).
[7] D. K. Schwartz, C. M. Knobler, and A. Bruinsma, Phys. Rev. Lett. **73**, 2841 (1994).
[8] A. Relini, F. Ciuchi, and R. Rolandi, J. Phys. II **5**, 1209 (1995).
[9] M. L. Kurnaz and D. K. Schwartz, Phys. Rev. E **56**, 3378 (1997).
[10] G. T. Shahin, Ph.D. thesis, University of Pennsylvania, 1986.
[11] C. F. Brooks, G. G. Fuller, C. W. Frank, and C. R. Robertson, Langmuir **15**, 2450 (1999).
[12] J. Ding, H. E. Warriner, and J. A. Zasadzinski, Phys. Rev. Lett. **88**, 168202 (2002).
[13] J. Q. Ding, H. E. Warriner, J. A. Zasadzinski, and D. K. Schwartz, Langmuir **18**, 2800 (2002).
[14] T. M. Fischer, J. Fluid Mech. **498**, 123 (2004).
[15] A. J. Levine, T. B. Liverpool, and F. C. MacKintosh, e-print cond-mat/0303095.
[16] A. K. Doolittle, J. Appl. Phys. **22**, 1471 (1951).
[17] A. K. Doolittle and D. B. Doolittle, J. Appl. Phys. **28**, 901 (1957).
[18] M. Sickert and F. Rondelez, Phys. Rev. Lett. **90**, 126104 (2003).
[19] B. A. Grzybowski, N. Bowden, F. Arias, H. Yang, and G. M.-Whitesides, J. Phys. Chem. **105**, 404 (2001).
[20] J. N. Israelachvili, *Intermolecular and Surface Forces* (Academic, London, 1992).
[21] The units of surface viscosity in the literature are in surface-poise or poise-cm, both of which are equivalent to g/s. The SI equivalent is (mN s)/m.
[22] C. A. Helm, H. Mohwald, K. Kjaer, and J. Als-Nielsen, Biophys. J. **52**, 381 (1987).
[23] H. Mohwald, Annu. Rev. Phys. Chem. **41**, 441 (1990).

[24] H. McConnell, Annu. Rev. Phys. Chem. **42**, 171 (1991).
[25] V. M. Kaganer, H. Mohwald, and P. Dutta, Rev. Mod. Phys. **71**, 779 (1999).
[26] K. Y. C. Lee, A. Gopal, A. Von Nahmen, J. A. Zasadzinski, J. Majewski, G. S. Smith, P. B. Howes, and K. Kjaer, J. Chem. Phys. **116**, 774 (2002).
[27] F. Bringezu, J. Ding, G. Brezesinski, and J. A. Zasadzinski, Langmuir **17**, 4641 (2001).